Pulse Delay Time Statistics in a Superradiant Laser with Calcium Atoms

Torben Laske, Hannes Winter, and Andreas Hemmerich*
Institut für Laser-Physik and Zentrum für Optische Quantentechnologien, Universität Hamburg, D-22761 Hamburg, Germany

(Received 23 March 2019; published 3 September 2019)

Cold samples of calcium atoms are prepared in the metastable $^3P_1$ state inside an optical cavity resonant with the narrow band (375 Hz) $^1S_0 \rightarrow {}^3P_1$ intercombination line at 657 nm. We observe a superradiant emission of hyperbolic secant shaped pulses into the cavity with an intensity proportional to the square of the atom number, a duration much shorter than the natural lifetime of the $^3P_1$ state, and a delay time fluctuating from shot to shot in excellent agreement with theoretical predictions. Our incoherent pumping scheme to produce inversion on the $^1S_0 \rightarrow {}^3P_1$ transition should be extendable to allow for continuous wave laser operation.

DOI: 10.1103/PhysRevLett.123.103601

Conventional lasers typically operate in the so-called *good cavity* limit, where the resonance bandwidth of the feedback cavity is by far more narrow than the spectral width of the gain profile. The achievable emission bandwidth is presently approaching fundamental limitations by intrinsic thermal fluctuations of the cavity materials [1–3], which is one of the obstacles for further improvements of the precision of atomic clocks [4]. An alternative approach to circumvent these limitations relies on the use of an ultranarrow bandwidth gain material, as provided by two-electron atoms like calcium or strontium, in combination with a comparatively large cavity bandwidth. In this so-called *bad cavity* regime, the average intracavity photon number can be kept small and even well below unity such that the intracavity field cannot establish coherence, as in the good cavity regime. Here, it is rather the long-lived atomic polarization providing the phase memory necessary to form coherence by superradiant emission, with the result of a sensitivity to technical noise sources reduced by many orders of magnitude. Bad cavity lasers, also referred to as superradiant lasers, are a subject of ongoing theoretical [5–8] and experimental [9,10] research. In the recent past, superradiant lasing has undergone a renaissance in connection with the use of ultranarrow band intercombination lines of alkaline-earth atoms [8,11–14], which could provide extremely low emission bandwidths in the submillihertz regime.

Superradiant emission of an inverted system in free space has been studied since the fifties [15–22] followed by first observations in the optical domain in the seventies [23–25]. More recently, a new line of research has been concerned with the collective light scattering by dense ultra-cold samples of atoms in free space as well as inside optical cavities [26–29]. On a macroscopic level, a completely inverted system represents an unstable equilibrium. Its decay is triggered by microscopic quantum fluctuations, which translate into macroscopic shot to shot delay time fluctuations of classical superradiant light pulses. This phenomenon has been theoretically studied [22,30], but a quantitative comparison with experiments is yet missing. In this Letter we report the first pulsed superradiant laser with bosonic calcium (^{40}Ca) atoms. This is achieved by providing inversion with respect to the narrow band ($\Gamma/2\pi = 375$ Hz) $^1S_0 \rightarrow {}^3P_1$ intercombination line at 657 nm [31]. Hyperbolic secant shaped pulses are observed with a temporal delay that fluctuates from shot to shot, thus reflecting the initial quantum stage of the pulse evolution. The stochastic nature of superradiance is studied quantitatively by measuring the pulse delay time statistics for different numbers of participating emitters. We find excellent agreement with an analytical model that does not require the adjustment of fitting parameters. In contrast to a recent first experimental realization of superradiant lasing with strontium atoms [13,14], we use an incoherent pump process to provide inversion, which should allow an extension to continuous wave operation.

The preparation of inversion on the $^1S_0 \rightarrow {}^3P_1$ transition at 657 nm proceeds in the two steps illustrated in Fig. 1:

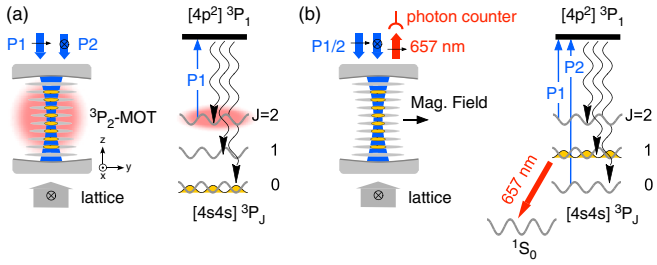

FIG. 1. The two steps for preparation of inversion are sketched in (a) and (b). An intracavity lattice at 800.8 nm is formed with linear polarization along the x axis. $P1$ and $P2$ denote optical pumping lasers with linear polarizations along the y axis and x axis, operating at 432 nm and 429 nm, respectively. Laser emission at 657 nm is recorded with a photon counter.

initially, a magneto-optic trap ($^3P_2$-MOT), using the 57 kHz $^3P_2 \rightarrow {}^3D_3$ closed cycle transition at 1978 nm, prepares about 2×10^8 atoms at a temperature of 200 μK in the $^3P_2$ state. Details are found in Refs. [32–35]. As sketched in Fig. 1(a), the cold cloud of atoms produced in the $^3P_2$-MOT is superimposed upon a longitudinal mode of a linear cavity with a finesse $F = 2200$, a free spectral range of 2.5 GHz, a transmission resonance bandwidth $\kappa/\pi = 2260$ kHz, and a $(1/e^2)$ waist $w_0 = 190$ μm (for light at a wavelength of 657 nm). The cavity exhibits a Purcell factor $\eta \equiv (24F/\pi k^2 w_0^2) = 0.0051$ with $k = 2\pi/657$ nm [36]. A laser beam at 800.8 nm, i.e., the magic wavelength [37] for the $^1S_0 \rightarrow {}^3P_1$, $m = 0$ transition for $\sigma_\pm$ polarized light, is coupled to the cavity to create an intracavity optical lattice potential. A laser beam ($P1$) at 432 nm, aligned with the cavity mode with a waist of $w_0 = 100$ μm, pumps atoms within a small tube around the lattice axis into the $^3P_0$ state, where they are trapped in the lattice potential. The intensity of this beam is low such that only atoms passing the pump volume at low velocities, hence interacting with this beam for a sufficiently long amount of time, are pumped [38–40]. Thus, up to several 10^5 atoms in the $^3P_0$ state are typically trapped in the lattice potential with a temperature of about 100 μK and a peak density of 10^{10} cm^{-3}. Adjustment and technical fluctuations of the atom number are discussed in more detail in Ref. [41]. The trapped atom cloud extends over 2.5 mm along the lattice axis corresponding to several thousand lattice sites with an average population of a single pancake-shaped site of several ten atoms. Hence, contact interaction between atoms may be completely neglected. Also, in contrast to superradiant scattering in Bose-Einstein condensates, at these low densities, no complex light propagation dynamics occurs [45].

In a second phase of the preparation protocol, sketched in Fig. 1(b), the $^3P_2$-MOT is switched off, a homogeneous magnetic field of a few Gauss is oriented along the y axis and an additional laser at 429 nm ($P2$), also adjusted along the cavity axis, however linearly polarized in the x direction, is activated during 50 μs, in order to rapidly pump all $^3P_0$ atoms into the $^3P_1$ state. According to a rate equation model of the optical pumping dynamics, only about 25% of the $^3P_1$ atoms are transferred into the relevant $m = 0$ state, which acts as the upper laser level. The applied homogeneous magnetic field shifts the magnetic $m = \pm 1$ atoms several MHz out of resonance with the cavity. The lattice potential provides the same light shift for the $^3P_1$, $m = 0$ and $^1S_0$ states [46] and operates well within the Lamb-Dicke regime, such that the Doppler effect is suppressed along the z direction to the first order. Hence, if the cavity is tuned into resonance, superradiant emission of a large fraction of the $^3P_1$, $m = 0$ atoms can arise. Precisely controlled tuning of the laser cavity resonance with respect to the $^1S_0 \rightarrow {}^3P_1$ transition frequency is achieved by actively stabilizing the cavity to a diode laser beam at

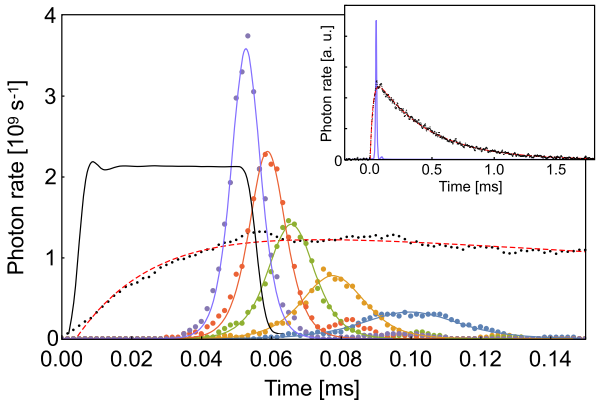

FIG. 2. The inset (upper right corner) compares the natural noncooperative exponential decay (black dots) with the case when a short (≈10 μs) superradiant pulse is emitted (blue graph). The red dashed line is a fit with two exponential functions as explained in the text. In order to present both graphs in the same plot, their vertical axes are scaled differently. The main panel shows superradiant light pulses for atom numbers $N_0 = 12\,800, 19\,700, 26\,500, 34\,000, 42\,300$ from right to left. The solid black line indicates the pump pulse that acts to populate the $^3P_1$ state. The black dots, modeled by the dashed red line graph, repeat the natural decay curve of the inset.

780.2 nm locked to a Doppler-free resonance of rubidium atoms and sent through a electro-optic fiber modulator (EOFM) tunable between 400 and 1000 MHz. Adjusting the EOFM driving frequency, the cavity resonance is adjusted to match the atomic resonance at 657 nm (see the Supplemental Material [41] for details). The lattice frequency is actively stabilized to the longitudinal mode of the laser cavity that is closest to the magic wavelength, i.e., less than half of the free spectral range, which amounts to 1.25 GHz.

After preparing an inverted sample of several 10^4 atoms in the metastable $^3P_1$, $m = 0$ state, we observe a superradiant pulsed emission (linearly polarized along the y axis), which brings a significant fraction of the atoms into the $^1S_0$ ground state in a time much shorter than the natural life time of the $^3P_1$ state. The inset in the upper right corner of Fig. 2 compares the natural noncooperative exponential decay with an observed life time of 420 μs (black dots approximated by red dashed line) with the case when a short (≈10 μs) superradiant pulse is emitted (blue graph). In both cases a sample of metastable calcium atoms in the $^3P_1$ state is prepared with the cavity tuned into resonance with the $^1S_0 \rightarrow {}^3P_1$ transition only in the latter case. The noncooperative emission into free space is observed in the xy plane at an angle of 22.5° with respect to the y axis. The main panel of Fig. 2 is enlarged to highlight the first 150 μs showing superradiant light pulses with five different peak photon numbers and peak times. Each trace represents a single-shot implementation. The observed pulses can be well fitted with hyperbolic secants derived from a

semiclassical analytical model outlined below and in more detail in Ref. [41]. Two parameters are determined from these fits: the number of collectively emitting atoms N_0 and the time t_p when the pulse attains its maximum. For the shown pulses, $N_0 = 12\,800, 19\,700, 26\,500, 34\,000, 42\,300$ from right to left. Besides N_0 and t_p the hyperbolic secant fit model comprises the Purcell factor of the cavity η, the natural linewidth Γ of the used transition, and the bunching parameter B. The latter accounts for a reduction of the atom-cavity coupling strength resulting from the fact that the period of the atomic grating held by the magic lattice (800.8 nm) and that of the intracavity standing wave at the emission wavelength (657.5 nm) are not commensurate. For a homogeneous atomic distribution the value of B should be $1/2$, while our experimental data are best described by $B \approx 0.65$. This value, which matches with a more elaborate analysis in Ref. [47], is used in all fits. Taking into account the losses between the cavity and the photon counter and the detector efficiency, the specified counting rate is calibrated to indicate the total rate of photons leaving the cavity through both mirrors. A counting rate of 10^9 s^{-1} corresponds to an intracavity photon number $n \approx 70$.

A notable observation is that the average pulse peak time $\bar{t}_p$ grows with decreasing N_0, while for fixed N_0 the individually measured values of t_p fluctuate around $\bar{t}_p$. In order to determine $\bar{t}_p$ and its dependence on the atom number N_0, we recorded several thousand pulses and plotted the averages over the observed pulse peak times $\bar{t}_p$ versus N_0 using a binning $N_0 \pm 2500$ for the atom number, such that each data point in the blue trace in Fig. 3(a) represents several hundred pulses with nearly equal atom number. The error bars depict the standard deviations Δt_p, which, similarly as $\bar{t}_p$ itself, are observed to decrease for increasing N_0. In the red trace of (a), we subtract the analytical model $\bar{t}_d = (N_0 \eta B \Gamma)^{-1} \log(N_0)$, discussed below and in Ref. [41]. This model assumes the instantaneous formation of complete inversion at some initial time t_0. For the choice $B = 0.65$, we remain with a practically constant temporal offset of 24 μs (red dashed line), which represents the time t_0 when inversion is effectively formed by the pump pulse. The blue dotted line graph shows $\bar{t}_d + t_0$. Apart from the choice of B, this procedure does not involve any parameter adjustment, thus confirming the validity of the theoretical description.

In our experiment, according to the scheme illustrated in Fig. 1(b), the upper laser level $^3P_1$, $m = 0$ is in fact not instantaneously pumped, but rather loaded at a rate $R(t) \equiv (N_0/\tau_p) e^{-t/\tau_p}$, where τ_p denotes the $1/e$ time for this process (see Fig. 2). The corresponding population of the upper laser level is $N(t) = \int_0^t ds R(s) = N_0(1 - e^{-t/\tau_p})$. The limited intensity available for the lasers $P1$ and $P2$ in Fig. 1(b) gives rise to $\tau_p \approx 21$ μs. An analysis deferred to Ref. [41] shows that the pulse peak time $\bar{t}_p$ can be nevertheless written as a sum $\bar{t}_p = t_0 + \bar{t}_d$, where t_0 only depends on τ_p but not on N_0, and $\bar{t}_d$ denotes the mean pulse delay time found for a scenario of instantaneous pumping, i.e., with $R(t) = 0$ and the upper laser level initially populated by N_0 atoms at time t_0.

One may go beyond the determination of $\bar{t}_p$ and Δt_p and consider the full pulse delay time probability distribution. Restricting ourselves to two different atom numbers $N_1 = 3 \times 10^4$ and $N_2 = 1.5 \times 10^4$ we proceed as follows: the time axis is partitioned into time windows of 5 μs

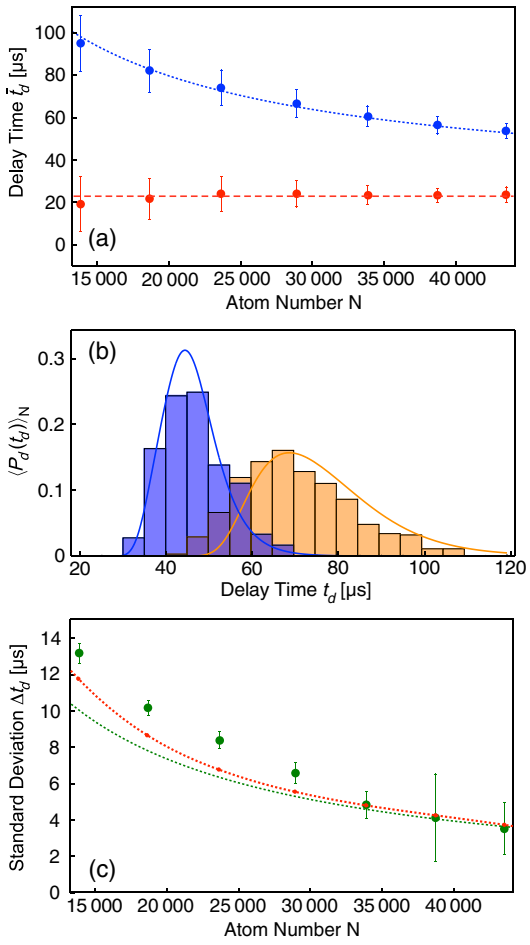

FIG. 3. (a) Pulse delay time versus N_0. The blue data points denote the observed pulse peak times $\bar{t}_p$. The red points arise, if the analytical model $\bar{t}_d$ is subtracted from the blue points leaving a small constant rest t_0. The blue dotted line graph shows $\bar{t}_d + t_0$. (b) Observed (histograms) and theoretically predicted (solid line graphs) delay time probability distributions (plotted versus t_d, i.e., with t_0 subtracted) for pulses with atom numbers around $N_1 = 3 \times 10^4$ (blue) and $N_2 = 1.5 \times 10^4$ (yellow). (c) The green disks show the standard deviations of the observed pulse delay time versus the atom number N_0 for a partition dividing the N_0 axis into seven sectors. The error bars show the corresponding standard deviations of the mean. The dashed green line shows the theoretical expectation according to $P_d(t_d)$. The dashed red line in addition includes a systematic contribution due to the use of a finite partition.

width and the number of pulses with atom numbers in the interval $\mathcal{N}_i \equiv [N_i - \delta N, N_i + \delta N], i \in \{1,2\}$ with $\delta N = 5 \times 10^3$ falling into each time window is counted. The histograms (normalized to unity) thus obtained for the two choices N_i, $i \in \{1,2\}$ are plotted in Fig. 3(b). Our theoretical model predicts a delay time distribution $P_d(t_d) \equiv N_0^2 B\eta\Gamma e^{-N_0 B\eta\Gamma t_d} \exp(-N_0 e^{-N_0 B\eta\Gamma t_d})$. The solid line graphs in Fig. 3(b) show $\langle P_d(t_d)\rangle_{N_0 \in \mathcal{N}_i}$ where the bracket denotes averaging over all values of N_0 within the interval $\mathcal{N}_i$. Very good agreement between the observations and our analytical model is found, which does not rely on the adjustment of fit parameters. Finally, in Fig. 3(c), the observed standard deviations of the pulse delay times as given by the error bars in Fig. 3(a) are plotted versus the atom number N_0 (green disks) and compared to the theoretical expectations according to $P_d(t_d)$ (dashed green line graph). Again, no parameter adjustment is applied. The observed fluctuations exceed the theoretical predictions for small atom numbers. A smaller part of this disagreement can be attributed to the choice of a relatively coarse partition in Fig. 3(c), used to ensure that each atom number class comprises a large number of pulses. The dashed red line graph shows the theoretically expected standard deviations including this partition-dependent contribution. See the Supplemental Material [41] for details. The remaining discrepancy between theory and experiment for small atom numbers might be due to the correspondingly large pulse delay times, which should increase possible contributions from technical fluctuations. Note also that we do not observe pulses with $N_0 < 10^4$, which indicates the presence of a possible threshold that could be attributed to inhomogeneous line broadening (see the Supplemental Material [41]).

We now briefly summarize the theoretical model used to determine the delay time probability distribution $P_d(t_d)$ and the mean delay time $\bar{t}_d$ for the case of instantaneous formation of inversion. The extension to the case of noninstantaneous pumping is deferred to the Supplemental Material [41]. Our starting point is a modified semiclassical laser equation for N_0 two-level atoms all occupying the excited state at time $t = 0$ [as e.g., in Eq. (8.8) on page 230 of Ref. [48]]. We account for the fact that for a sample of N_0 atoms at positions z_a along the axis of the lasing cavity mode, which is associated with an intensity distribution $\cos^2(kz_a)$, the effective coupling strength is reduced by the bunching parameter $B \equiv (1/N_0)\sum_a \cos^2(kz_a)$. For $0 < t \ll \Gamma^{-1}$, a solution for the intracavity photon number is given by the pulse $n(t) = (\eta B\Gamma/8\kappa)N_0^2 \operatorname{sech}^2[\frac{1}{2}N_0\eta B\Gamma(t - t_d)]$ with $\operatorname{sech}(z)$ denoting the hyperbolic secant. Setting $t = 0$ and $n_0 \equiv n(0)$ leads to $n_0 \approx (\eta B\Gamma/2\kappa)N_0^2 e^{-N_0\eta B\Gamma t_d}$ and hence $dn_0 = -N_0\eta B\Gamma n_0 dt_d$. The delay time t_d is determined by the initial photon number at $t = 0$, which can be evaluated as follows. The mean rate of spontaneous photons released into the cavity at times much shorter than $(N_0\eta\Gamma)^{-1}$ is $R_{\mathrm{sp}} = N_0\eta B\Gamma$, which is compensated by the photon loss rate 2κ to yield the steady state photon number $\bar{n}_0 = (R_{\mathrm{sp}}/2\kappa)$. The rate R_{sp} corresponds to an average time between successive spontaneous photons $\Delta t_{\mathrm{sp}} = (N_0\eta B\Gamma)^{-1}$, which is on the order of 10 μs. Assuming that $\bar{n}_0$ equals the initial photon number n_0 at $t = 0$, we may evaluate the mean delay time as $\bar{t}_d = (N_0\eta B\Gamma)^{-1}\log(N_0)$. We may go one step further and calculate the delay time distribution. Note that $\bar{n}_0$ is on the order of 10^{-2} and hence much smaller than unity. For this case the probability for N_0 atoms to spontaneously emit n_0 photons into the cavity, generally given by a binomial distribution, can be well approximated by an exponential. Hence, the probability of initially finding n_0 photons in the cavity is given by the normalized distribution $P_i(n_0) \equiv (1/\bar{n}_0)\exp(n_0/\bar{n}_0)$, which reproduces the previously determined steady state photon number $\bar{n}_0$. With the expressions of t_d and dt_d/dn_0 as functions of n_0, discussed above, one finds $P_i(n_0)dn_0 = P_d(t_d)dt_d$, where $P_d(t_d)$ is the delay time distribution used in Fig. 3(b). It is worthwhile to note that the expressions obtained for $P_d(t_d)$ and $\bar{t}_d$ are in accordance with reduced expressions, merely depending on N_0 and Γ, reported in Ref. [22] to model superradiance for a homogeneous atomic sample in free space with no cavity present.

In contrast to Ref. [14], an incoherent pump process is used in our work to provide inversion, which should allow for an extension to continuous wave operation. Two different strategies into this direction could be followed. One option could be to use 657 nm radiation to re-excite ground state atoms to $^3P_1$, $m = \pm 1$ and subsequently optically pump them with the help of 430 nm radiation to $^3P_1$, $m = 0$. A second option is to enable the loading of the magic lattice with $^3P_2$ atoms directly from the $^3P_2$-MOT. At present, this is not possible, because the magic lattice wavelength leads to a large negative light shift of the upper MOT level $^3D_3$, such that the MOT frequency is tuned to the blue side of the atomic resonance and hence lattice loading is impeded. This could be counteracted by an additional laser that selectively provides a compensating positive light shift to the $^3D_3$ state. Similar results as obtained in the present Letter should also be possible for the $^1S_0 \rightarrow {}^3P_0$ transition. This transition can be endowed with an finite linewidth in the subhertz range adjusted by adding a small admixture of the $^3P_1$ state to $^3P_0$ by means of a homogeneous magnetic field of a few Gauss [49]. This could give rise to a superradiant laser with an adjustable extremely narrow bandwidth. Note that in this case the extension to continuous operation is straightforward, since the $^3P_0$ state can be continuously loaded from the $^3P_2$-MOT, as already shown in this Letter.

This work was partially supported by DFG-He2334/15.1. We thank Claus Zimmermann for useful discussions.

*hemmerich@physnet.uni-hamburg.de

[1] B. C. Young, F. C. Cruz, W. M. Itano, and J. C. Bergquist, Phys. Rev. Lett. **82**, 3799 (1999).

[2] T. Kessler, C. Hagemann, C. Grebing, T. Legero, U. Sterr, F. Riehle, M. J. Martin, L. Chen, and J. Ye, Nat. Photonics **6**, 687 (2012).

[3] D. G. Matei, T. Legero, S. Häfner, C. Grebing, R. Weyrich, W. Zhang, L. Sonderhouse, J. M. Robinson, J. Ye, F. Riehle, and U. Sterr, Phys. Rev. Lett. **118**, 263202 (2017).

[4] A. D. Ludlow, M. M. Boyd, J. Ye, E. Peik, and P. O. Schmidt, Rev. Mod. Phys. **87**, 637 (2015).

[5] M. Lax, in *Physics of Quantum Electronics*, edited by P. L. Kelley, B. Lax, and P. E. Tannenwald (McGraw-Hill, New York, 1966).

[6] H. Haken, *Laser Theory* (Springer-Verlag, Berlin, 1984).

[7] F. Haake, M. I. Kolobov, C. Fabre, E. Giacobino, and S. Reynaud, Phys. Rev. Lett. **71**, 995 (1993).

[8] D. Meiser, J. Ye, D. R. Carlson, and M. J. Holland, Phys. Rev. Lett. **102**, 163601 (2009).

[9] S. J. M. Kuppens, M. P. van Exter, and J. P. Woerdman, Phys. Rev. Lett. **72**, 3815 (1994).

[10] J. G. Bohnet, Z. Chen, J. M. Weiner, D. Meiser, M. J. Holland, and J. K. Thompson, Nature (London) **484**, 78 (2012).

[11] J. Chen and X. Chen, in *Proceedings of the 2005 IEEE International Frequency Control Symposium and Exposition, 2005* (IEEE, 2005), https://doi.org/10.1109/FREQ.2005.1574003.

[12] J. Chen, Chin. Sci. Bull. **54**, 348 (2009).

[13] M. A. Norcia and J. K. Thompson, Phys. Rev. X **6**, 011025 (2016).

[14] M. A. Norcia, M. N. Winchester, J. R. K. Cline, and J. K. Thompson, Sci. Adv. **2**, e1601231 (2016).

[15] R. H. Dicke, Phys. Rev. **93**, 99 (1954).

[16] V. Ernst and P. Stehle, Phys. Rev. **176**, 1456 (1968).

[17] N. E. Rehler and J. H. Eberly, Phys. Rev. A **3**, 1735 (1971).

[18] R. Bonifacio, P. Schwendimann, and F. Haake, Phys. Rev. A **4**, 302 (1971).

[19] F. Haake and R. Glauber, Phys. Rev. A **5**, 1457 (1972).

[20] R. Bonifacio and L. A. Lugiato, Phys. Rev. A **11**, 1507 (1975).

[21] R. Glauber and F. Haake, Phys. Rev. A **13**, 357 (1976).

[22] M. Gross and S. Haroche, Phys. Rep. **93**, 301 (1982).

[23] N. Skribanowitz, l. P. Herman, J. C. MacGillivray, and M. S. Feld, Phys. Rev. Lett. **30**, 309 (1973).

[24] M. Gross, C. Fabre, P. PiIlet, and S. Haroche, Phys. Rev. Lett. **36**, 1035 (1976).

[25] Ph. Cahuzac, H. Sontag, and P. E. Toschek, Opt. Commun. **31**, 37 (1979).

[26] S. Inouye, T. Pfau, S. Gupta, A. P. Chikkatur, A. Görlitz, D. E. Pritchard, and W. Ketterle, Nature (London) **402**, 641 (1999).

[27] S. Slama, S. Bux, G. Krenz, C. Zimmermann, and Ph. W. Courteille, Phys. Rev. Lett. **98**, 053603 (2007).

[28] H. Keßler, J. Klinder, M. Wolke, and A. Hemmerich, Phys. Rev. Lett. **113**, 070404 (2014).

[29] J. H. Müller, D. Witthaut, R. le Targat, J. J. Arlt, E. S. Polzik, and A. J. Hilliard, J. Mod. Opt. **63**, 1886 (2016).

[30] F. Haake, J. W. Haus, H. King, G. Schröder, and R. Glauber, Phys. Rev. A **23**, 1322 (1981).

[31] F. Riehle, *Frequency Standards, Basics and Applications* (Wiley-VCH, Weinheim, 2004).

[32] J. Grünert and A. Hemmerich, Appl. Phys. B **73**, 815 (2001).

[33] J. Grünert and A. Hemmerich, Phys. Rev. A **65**, 041401(R) (2002).

[34] D. Hansen, J. Mohr, and A. Hemmerich, Phys. Rev. A **67**, 021401(R) (2003).

[35] D. Hansen and A. Hemmerich, Phys. Rev. Lett. **96**, 073003 (2006).

[36] E. M. Purcell, Phys. Rev. **69**, 37 (1946).

[37] H. Katori, M. Takamoto, V. G. Pal'chikov, and V. D. Ovsiannikov, Phys. Rev. Lett. **91**, 173005 (2003).

[38] C. Y. Yang, P. Halder, O. Appel, D. Hansen, and A. Hemmerich, Phys. Rev. A **76**, 033418 (2007).

[39] P. Halder, C.-Y. Yang, and A. Hemmerich, Phys. Rev. A **85**, 031603(R) (2012).

[40] P. Halder, H. Winter, and A. Hemmerich, Phys. Rev. A **88**, 063639 (2013).

[41] See Supplemental Material at http://link.aps.org/supplemental/10.1103/PhysRevLett.123.103601 for the theoretical modeling, experimental procedures, and data analysis protocols, which includes Refs. [42–44].

[42] C. Cohen-Tannoudji, J. Dupont-Roc, and G. Grynberg, *Atom-Photon Interactions: Basic Processes and Applications* (Wiley-VCH, New York, 1992).

[43] H. Tanji-Suzuki, I. D. Leroux, M. H. Schleier-Smith, M. Cetina, A. T. Grier, J. Simon, and V. Vuletic, Adv. At. Mol. Opt. Phys. **60**, 201 (2011).

[44] A. Schoof, J. Grünert, S. Ritter, and A. Hemmerich, Opt. Lett. **26**, 1562 (2001).

[45] L. Deng, M. G. Payne, and E. W. Hagley, Phys. Rev. Lett. **104**, 050402 (2010).

[46] C. Degenhardt, H. Stoehr, U. Sterr, F. Riehle, and Ch. Lisdat, Phys. Rev. A **70**, 023414 (2004).

[47] J. Hu, W. Chen, Z. Vendeiro, H. Zhang, and V. Vuletić, Phys. Rev. A **92**, 063816 (2015).

[48] D. Meschede, *Optics, Light and Lasers* (Wiley-VCH, Berlin, 2004).

[49] A. V. Taichenachev, V. I. Yudin, C. W. Oates, C. W. Hoyt, Z. W. Barber, and L. Hollberg, Phys. Rev. Lett. **96**, 083001 (2006).